International Journal of Mechanical Sciences 314 (2026) 111297

Contents lists available at ScienceDirect

International Journal of Mechanical Sciences

journal homepage: www.elsevier.com/locate/ijmecsci

A refined Gibson-Ashby model for functionally graded honeycombs with random irregularities

M.J. Beigrezaee [a], S.K. Jalali [a], D. Misseroni [b], N.M. Pugno [a,c,*]

[a] Mechano-X labs, Department of Civil, Environmental and Mechanical Engineering, University of Trento, Italy
[b] Laboratory for the Design of Reconfigurable Metamaterials & Structures, Department of Civil, Environmental and Mechanical Engineering, University of Trento, Italy
[c] School of Engineering and Materials Science, Queen Mary University of London, Mile End Road, London E1 4NS, UK

ARTICLE INFO

Keywords:
Functionally graded
Gibson-ashby model
Irregular lattice structures
Porosity
Honeycombs
Additive manufacturing

ABSTRACT

Honeycomb lattices are widely used as lightweight architected materials, and their mechanical behavior is strongly influenced by unit-cell wall thickness and geometric configuration. Inspired by natural cellular structures, predicting the elastic response of honeycombs with wall-thickness grading and geometric irregularities remains challenging. This study refines the Gibson-Ashby equation for predicting the elastic modulus of honeycombs by introducing two correction factors, κ and η, accounting for functionally graded (FG) wall thickness variations and random irregularities, respectively, i.e., (relative modulus) = $\kappa\eta C$ (relative density)^n. Analytical expressions based on Timoshenko beam theory are extended to FG architectures, providing a stepwise formulation for relative density and elastic modulus variations along the FG direction. This yields a closed-form expression for the effective relative elastic modulus of FG honeycombs, validated by finite element (FE) simulations. Here, κ is calibrated over a broad range of linear and nonlinear wall thickness gradients. Since closed-form formulations for periodic lattices cannot capture random irregularities, η is fitted to an extensive set of FE simulations with random designs. These correction factors are presented as design charts covering hexagonal, square, and triangular honeycombs. Additively manufactured samples produced by 3D printing are tested to validate the predictions and quantify real-world imperfections. This framework provides a direct and computationally efficient means to estimate the elastic modulus of graded and irregular 2D lattices without requiring full numerical homogenization or experiments. The study introduces a unified correction-based approach that bridges analytical cellular-material models with the complexity of natural and fabricated honeycombs.

1. Introduction

Recent advances in digital and additive manufacturing have significantly expanded the design space for cellular solids, enabling the fabrication of complex architectures with tailored properties [1]. Cellular solids encompass a broad class of engineered porous materials. Honeycombs, a subset of cellular solids, are commonly formed by in-plane repetition of a two-dimensional unit cell with extrusion along the third dimension [2]. Conventional honeycomb designs with hexagonal, triangular, and square unit cells, have been widely studied due to their well-defined periodicity, which simplifies both manufacturing and modeling [3]. However, non-periodic and irregular honeycomb architectures — where structural variations arise from graded wall thickness or random irregularities in unit cell geometry — have received significantly less attention despite their potential advantages. Natural systems, such as bones, frequently exploit both graded and irregular architectures to enhance mechanical efficiency, motivating the exploration of such designs for engineered structures. Expanding beyond conventional periodic designs allows for optimized honeycombs with superior mechanical performance [4], particularly in lightweight applications such as aerospace and automotive engineering, as well as biomedical applications [5]. Historically, the fabrication of non-periodic structures was constrained by manufacturing limitations, leading to a preference for uniform, periodic honeycombs. However, recent developments in additive manufacturing have overcome these constraints, enabling precise control over spatial variations in geometry and unlocking new opportunities for functional grading (FG) and random irregularity in honeycombs [4,6].

For periodic cellular solids with a well-defined repeating unit cell, the relationship between mechanical properties and relative density can be derived through structural mechanics analysis [7–17]. Under simplified assumptions, the structural analysis may result in a

* Corresponding author.
E-mail addresses: nicola.pugno@unitn.it, pugno.dicam@unitn.it (N.M. Pugno).

https://doi.org/10.1016/j.ijmecsci.2026.111297
Received 29 September 2025; Received in revised form 29 December 2025; Accepted 20 January 2026
Available online 21 January 2026

closed-form expression similar to the power-law form of the classical Gibson-Ashby equation [2], where a mechanical property is evaluated as $C\times(\text{relative density})^n$. In such cases, direct comparison with analytical solutions allows for the determination of multiplier C and exponent n. However, when the simplified assumptions in structural mechanics analysis break down — such as in cases where the wall thickness-to-length ratio is large and shear-axial-bending coupling happens and the walls' overlaps in joints are not ignorable — the analytically derived equations (if exist) may not obey the simplified classical power-law form of the Gibson-Ashby equation. In these scenarios, the classical Gibson-Ashby equation is not able to accurately fit experimental and/or FE simulation results over a wide range of relative densities. Besides, when the structure lacks periodicity, the power-law equation may be empirically fitted to the data to obtain the most suitable values for C and n [18]. In some cases, the classical Gibson-Ashby power-law form fails to provide a reliable best-fit across a broad density range, necessitating modifications to the original form [19].

Given the effectiveness of FG microstructures, numerous studies have explored their potential to enhance the mechanical performance of cellular solids. The fundamental concept behind FG design is to introduce a controlled variation in microstructural parameters — such as cell wall thickness, pore size, or bulk material — to achieve optimized mechanical behavior. Compared to repetitive uniform structures, FG configurations offer significant advantages in tailored mechanical responses owing to functional material distribution [20]. Key investigations have demonstrated that FG designs can substantially improve kinetic energy absorption [21–24], reduce initial peak stress under impact loading [25], and enhance buckling collapse [26]. These findings make FG designs highly promising for various engineering applications from graded scaffolds [27–30] to microwave lenses [31].

The application of FG cellular solids as structural components, such as beams and plates, has been widely investigated. These studies have demonstrated how a controlled distribution of material along the thickness or length of a structural element can effectively tailor its mechanical response such as stability [32–34], and vibrations [35–38], ultimately leading to optimized structural designs. In such configurations, the mechanical properties vary spatially, making the structure inherently heterogeneous. The foundational approach in most of these studies relies on the Gibson–Ashby equation to establish a relationship between the relative density distribution and the corresponding variations in elastic properties within the structure [39,40]. However, a review of the literature indicates that in some cases, applying the Gibson–Ashby relation to define property variations within an FG cellular structure, based on spatial coordinates, has led to misunderstandings and misinterpretations by researchers [41]. This highlights the necessity for further investigations into the applicability and limitations of the Gibson–Ashby equation for FG cellular solids, ensuring its accurate use in structural modeling and optimization.

These limitations become especially relevant in modern bio-inspired cellular architectures where both FG and geometric irregularity coexist. Cellular architectures that combine functional grading with geometric irregularity are strongly rooted in bio-inspired design. Many natural systems evolve microstructures that vary gradually while incorporating controlled randomness, achieving exceptional mechanical efficiency. Trabecular bone exhibits coordinated density gradients together with inherent microstructural irregularity, enabling local stiffness tuning and load redistribution [42,43]. Wood and bamboo show stiffness and density gradients along the stem coupled with naturally irregular cellular patterns, providing high bending resistance under multi-axial loading [44]. These biological precedents demonstrate that combining grading and irregularity is an effective and naturally optimized strategy, not an artificial construction. Recent advances in additive manufacturing (AM) now allow engineers to reproduce these coupled natural mechanisms with high fidelity. Modern AM processes can intentionally introduce wall-thickness gradients while simultaneously generating geometric irregularities, either by design or as controlled manufacturing variations, enabling the fabrication of realistic FG irregular honeycombs.

Practical implementations of such structures already appear across several fields. Patient-specific bone scaffolds employ graded and irregular porosity to match the surrounding tissue stiffness, regulate local stress transfer, and promote osseointegration [42]. Protective sports and military helmet liners use FG and controlled irregularity to enhance impact-energy absorption and delay densification; recent studies show that irregularity increases toughness while functional grading manages the transmitted force [45]. Automotive crash boxes benefit from tailored wall-thickness distributions that maintain energy-absorption capability even when geometric imperfections are present, improving crashworthiness without increasing mass [46]. Lightweight aerospace components — such as morphing-wing cores and sandwich-panel lattices — use irregular FG microstructures to achieve high out-of-plane stiffness for load bearing while retaining in-plane compliance for morphing, weight reduction, and impact resistance [47]. More recently, graded and irregular honeycomb cores have also been explored in composite crashworthiness components, where they exhibit superior energy-absorption performance compared to uniform honeycombs [48]. These natural inspirations and practical engineered applications demonstrate that FG irregular honeycombs form a relevant and rapidly expanding class of manufacturable structures. The model developed in this work is therefore motivated by both biological evidence and current technological needs, providing a predictive framework capable of accurately capturing the combined effects of grading and irregularity in realistic honeycomb architectures. The study of random irregularities in honeycomb structures has been relatively limited, primarily due to the challenges associated with extending analytical formulations for periodic models to irregular, stochastic architectures. From an experimental standpoint, investigating the effects of random irregularities requires testing a large set of samples to capture the statistical distribution of structural imperfections, which can be costly and time-consuming. FE simulations have been employed as a practical alternative to reduce experimental costs while systematically analyzing the influence of randomness on mechanical properties. Findings indicate that by adjusting the degree of irregularity, it is possible to tailor mechanical performance for a given relative density. This offers a promising avenue for optimizing lattice structures where mechanical behavior can be fine-tuned without altering the overall material volume fraction [21,49–52].

This study directly addresses a critical gap in extending the classical Gibson-Ashby model to FG and randomly irregular honeycombs. A fundamental question in cellular solid design is whether the same power-law exponent n and multiplier C, calibrated for uniform periodic honeycombs, remain valid for FG and irregular architectures. Our findings demonstrate that applying the classical Gibson-Ashby equation without modification leads to significant errors in predicting the elastic modulus of such structures. However, we show that by introducing two correction factors — κ to account for FG variations and η to capture random irregularities — the classical framework can still provide accurate predictions without altering the exponent n. To facilitate practical implementation, κ and η are systematically calibrated through a combination of analytical modeling and extensive FE simulations, covering a wide spectrum of FG profiles (both linear and nonlinear) and degrees of randomness. The results are presented in the form of design charts, for conventional honeycomb designs namely, hexagonal (HEX), triangular (TRI), and square (SQ), offering a straightforward tool for engineers to optimize FG irregular honeycombs while exploiting existing knowledge of uniform periodic architectures. By bridging the gap between theoretical models and real-world applications, this work provides practical methodology for integrating FG and irregular lattice structures into advanced structural designs.

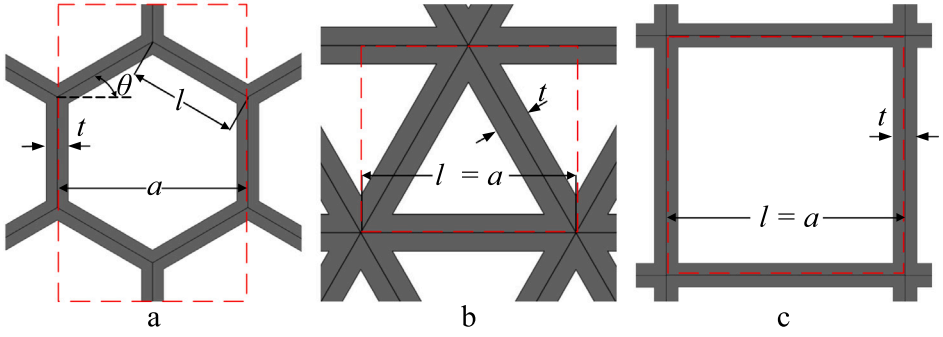

Fig. 1. Three different unit cells with their geometrical parameters (a) hexagonal (HEX), (b) triangular (TRI), and (c) square (SQ) unit cell.

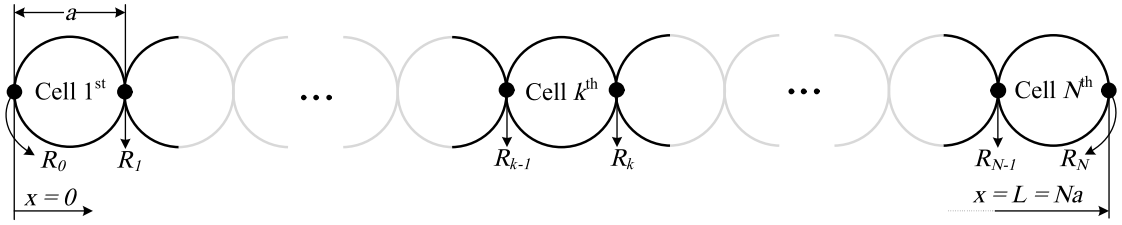

Fig. 2. The schematic of the graded honeycomb structure across FG direction, x. The dimensionless aspect ratio of the kth unit cell is the average of the aspect ratio of walls at the nodes on both sides.

2. Development of the model

2.1. Defining the geometry of FG honeycombs

Three different conventional unit cells have been selected for analysis i.e. HEX, TRI, and SQ [2]. Before introducing any random irregularities, the unit cells are assumed to be regular polygons with equal wall lengths l, as shown in Fig. 1. Note that for TRI and SQ lattices, the unit cell length is $a = l$ while for HEX it is $a = \sqrt{3}l$.

There are three ways to achieve a graded honeycomb structure. The first is by gradually changing the properties of the bulk material while keeping the honeycomb geometry unchanged. The second is by gradually changing the honeycomb wall length, while keeping the bulk material, and wall thickness fixed. The third is by gradually changing the thickness of the walls while keeping the bulk material, and honeycomb constant (constant unit cell length) fixed. Here, the third method is chosen because the first method encounters limitations in multi-material fabrication, while the second method introduces inevitable irregularities in the honeycomb structure, akin to the variations in pore size observed in irregular foams.

According to Fig. 2, a honeycomb structure with N unit cells of length a, and a total length of $L = Na$ has been assumed in which the thickness of walls located in the ith node between the cells has a certain thickness t_i. The dimensionless thickness (aspect ratio) of the wall at the ith node can be defined as $R_i = t_i/l$. In order to introduce the graded functionality to the honeycomb structure, the aspect ratio can be changed from R_0 at $x = 0$ to R_N at $x = L$ and the function of gradation is assumed as:

$$R_i = R_0 + \Delta R \left(\frac{i}{N}\right)^m, \tag{1}$$

in which $\Delta R = R_N - R_0$, and $i = 0, 1, 2, \ldots, N$. Here, the exponent m is chosen to be 1, 2, or 3 to capture both linear ($m = 1$) and nonlinear ($m \neq 1$) changes in the gradient. This allows for the consideration of various behaviors associated with the gradation in this study. Next, the average aspect ratio within the kth cell, $\bar{R}_k$, is defined by averaging the value of R at the $(k-1)$th, and kth nodes as,

$$\bar{R}_k = \frac{R_{k-1} + R_k}{2} = R_0 + \frac{\Delta R}{2N^m}\left((k-1)^m + k^m\right), \tag{2}$$

where $k = 1, 2, \ldots, N$. The elastic modulus of an FG honeycomb can be evaluated based on this step-wise variation of the aspect ratio through the length.

2.2. Relative density and elastic modulus of honeycombs

The relative density of a unit cell is a function of its constant aspect ratio, R, i.e., $\rho/\rho_0 = f(R)$, which can be evaluated by summing up the volume of all the walls within the unit cell divided to its total volume. However, the real relative density may be overestimated due to including the overlap part in the walls' joints which is higher for the bigger value of R. Excluding the overlaps in the joints, the exact value of the relative density for the honeycombs with HEX, TRI, and SQ unit cells can be evaluated as follows [53–56]:

$$\left(\frac{\rho}{\rho_0}\right)_{HEX} = \frac{2}{\sqrt{3}}R - \frac{1}{3}R^2, \tag{3a}$$

$$\left(\frac{\rho}{\rho_0}\right)_{TRI} = 2\sqrt{3}R - 3R^2, \tag{3b}$$

$$\left(\frac{\rho}{\rho_0}\right)_{SQ} = 2R - R^2, \tag{3c}$$

where ρ and ρ_0 are the density of lattice structure and its equivalent bulk material , respectively. Likewise, the relative elastic modulus of the unit cell is a function of its aspect ratio i.e. $E/E_0 = g(R)$. Employing structural analysis based on shear deformable Timoshenko beam theory, the relative elastic modulus for HEX, TRI, and SQ unit cells is calculated as follows [53–56]:

$$\left(\frac{E}{E_0}\right)_{HEX} = \frac{4R^3}{\sqrt{3}}\frac{1}{1 + (5.4 + 1.5\nu_0)R^2}, \tag{4a}$$

$$\left(\frac{E}{E_0}\right)_{TRI} = \frac{2R}{\sqrt{3}}\frac{1 + R^2}{1 + \frac{1}{3}R^2}, \tag{4b}$$

$$\left(\frac{E}{E_0}\right)_{SQ} = R, \tag{4c}$$

where E and ν are the elastic modulus and the Poisson's ratio of the lattice structure and the 0 subscription indicates the equivalent bulk material. The relative density and elastic modulus of a uniform

honeycomb with a fixed aspect ratio, R_u, is constant across the whole structure. They can be evaluated by setting $R = R_u$ in Eqs. (3) and (4). By contrast, in the FG honeycombs the aspect ratio R varies from R_0 to R_N according to Eq. (1). It results in a step-wise change along the FG direction, which is the x axis in this study. The relative density, $(\rho/\rho_0)^{(k)}$, of the kth unit cell of an FG honeycomb is calculated by substituting the average aspect ratio, $\bar{R}_k$, from Eq. (2) to Eq. (3):

$$\left(\frac{\rho}{\rho_0}\right)^{(k)}_{HEX} = \frac{2}{\sqrt{3}}\bar{R}_k - \frac{1}{3}\bar{R}^2, \tag{5a}$$

$$\left(\frac{\rho}{\rho_0}\right)^{(k)}_{TRI} = 2\sqrt{3}\bar{R} - 3\bar{R}^2, \tag{5b}$$

$$\left(\frac{\rho}{\rho_0}\right)^{(k)}_{SQ} = 2\bar{R} - \bar{R}^2. \tag{5c}$$

Similarly, the relative elastic modulus, $(E/E_0)^{(k)}$, is obtained by replacing R with $\bar{R}_k$ in Eq. (4):

$$\left(\frac{E}{E_0}\right)^{(k)}_{HEX} = \frac{4\bar{R}_k^3}{\sqrt{3}}\frac{1}{1+(5.4+1.5\nu_0)\bar{R}_k^2}, \tag{6a}$$

$$\left(\frac{E}{E_0}\right)^{(k)}_{TRI} = \frac{2\bar{R}_k}{\sqrt{3}}\frac{1+\bar{R}_k^2}{1+\frac{1}{3}\bar{R}_k^2}, \tag{6b}$$

$$\left(\frac{E}{E_0}\right)^{(k)}_{SQ} = \bar{R}_k. \tag{6c}$$

2.3. The approximation function for density and elastic modulus of FG honeycombs

Since the gradation of the aspect ratio is based on a power law with the exponent m (Eq. (1)), given the values of relative density and elastic modulus of unit cells by Eq. (5) and Eq. (6), one may fit an approximation function of the form $Ax^{\alpha m} + B$ on these values along the FG direction, x, as,

$$P(x) \approx Ax^{\alpha m} + B, \tag{7a}$$

$$A = \frac{P^{(N)} - P^{(1)}}{a^{\alpha m}((N-0.5)^{\alpha m} - 0.5^{\alpha m})}, \tag{7b}$$

$$B = P^{(1)} - (0.5a)^{\alpha m}A, \tag{7c}$$

in which $P(x)$ is either relative density or relative elastic modulus $(\rho(x)/\rho_0$ or $E(x)/E_0)$ and α is a calibrated parameter which can be evaluated by use of curve fitting method, illustrated in Fig. S1 and Fig. S2 in **Supplementary Information File** for different geometries. The calibrated parameter α has been calculated for a range of $R_0 < R_N < 0.5$. Note that during the fitting of $P(x)$, the properties of cells are assigned to their central x-coordinates. Besides, Eq. (7) is fitted so that it exactly passes through the relative properties of the first $(k = 1)$ and the last $(k = N)$ unit cell which are evaluated at $x = 0.5a$ and $x = (N - 0.5)a$, respectively. Given Eq. (7), it is possible to approximate a discontinuous FG honeycomb structure as a continuous graded medium. Fig. S3 and Fig. S4 in **Supplementary Information File** plot fitted approximation functions, Eq. (7) for relative density and elastic modulus, by setting $N = 20$ and considering a wide range of variation in wall aspect ratio, ranging from 0.05 to R = 0.25, while the corresponding calibrating parameter, α, is evaluated from the graphs in Fig. S1 and Fig. S2 in **Supplementary Information File**. Furthermore, to expand the range of grading variation in aspect ratio, three values of $m = 1$, 2, and 3 are also considered. Fig. S3 and Fig. S4, confirm the accuracy of the approximated functions introduced in Eq. (7). It is important to note that the fitting parameter α for the relative modulus of the honeycomb with a SQ unit cell is equal to 1, as indicated by Eq. (4c).

2.4. The effective properties of FG honeycombs

In the next step of homogenization, the FG honeycombs can be treated as a fully homogeneous medium by introducing *effective* properties denoted by a bar $(\bar{.})$. The effective density $\bar{\rho}$ can be described as the density of a fully homogeneous material whose mass is the same as the total mass of FG honeycombs with N cells while they have an identical apparent volume of $Nahb$ in which hb is the unit cell cross-section area perpendicular to the FG direction. The effective density can be evaluated as the average of the cells' density:

$$\frac{\bar{\rho}}{\rho_0} = \frac{1}{N}\sum_{k=1}^{N}\left(\frac{\rho}{\rho_0}\right)^{(k)}. \tag{8}$$

However, using the continuous approximation form of the graded relative density, Eq. (7), converts the summation of the previous formula to an integration form:

$$\frac{\bar{\rho}}{\rho_0} \approx \frac{\int_0^{Na}\left(\frac{\rho(x)}{\rho_0}\right)dx}{Na} = \frac{A(Na)^{(\alpha m)}}{\alpha m + 1} + B. \tag{9}$$

The FG honeycombs can be considered as N unit cells with the elastic modulus of $E^{(k)}$, $k = 1, \ldots, N$ which are connecting in series. The total elongation of the FG honeycombs under an applied load F_x is:

$$\delta_{graded} = \frac{F_x a}{hb}\sum_{k=1}^{N}\frac{1}{E^{(k)}}, \tag{10}$$

while the elongation of the equivalent fully homogeneous medium with a total length of Na is:

$$\bar{\delta} = \frac{F_x Na}{hb\bar{E}}. \tag{11}$$

Comparing Eqs. (10) and (11) one can define the effective relative elastic modulus as:

$$\frac{\bar{E}}{E_0} = \frac{N}{\sum_{k=1}^{N}\frac{1}{(E/E_0)^{(k)}}}, \tag{12}$$

where $(E/E_0)^{(k)}$ is calculated from Eq. (6). Similarly, the integration form related to the continuous approximated expression, Eq. (7), can be written as,

$$\frac{\bar{E}}{E_0} \approx \frac{Na}{\int_0^{Na}\frac{1}{(E(x)/E_0)}dx}. \tag{13}$$

Note that replacing Eq. (7) into Eq. (13) may need a numerical integration. The values of effective relative density and effective elastic modulus respectively calculated from Eqs. (8) and (12) have been illustrated in Fig. S5 to Fig. S7 in **Supplementary Information File** for a range of R_0 and R_N.

2.5. Definition of random irregularity

Various methods for introducing irregularity in honeycomb structures have been discussed in previous literature [21,51,52,57–59]. For the current study, the following equations have been applied to the initial coordinates of each node of the regular configuration $(x_{regular}, y_{regular})$ to find the updated coordinate $(x_{irregular}, y_{irregular})$ corresponding to the irregular structure:

$$\begin{aligned} x_{irregular} &= x_{regular} + \Lambda_1 \Delta l \cos(2\pi\Lambda_2) \\ y_{irregular} &= y_{regular} + \Lambda_1 \Delta l \sin(2\pi\Lambda_2), \end{aligned} \tag{14}$$

in which $0 \le (\Lambda_1$ and $\Lambda_2) \le 1$ represent random numbers, and Δ defines the degree of irregularity in the honeycomb structure. By applying Eq. (14), each node of the regular structure is randomly relocated within a circle with the radius Δl, as illustrated in Fig. 3. It is noteworthy that $\Delta = 0.5$ is the extreme value of the degree of randomness where there is a chance that some nodes may coincide, resulting in the removal

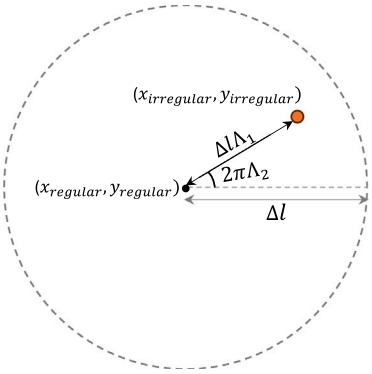

Fig. 3. Definition of random irregularity in honeycombs. By setting to random parameters, Λ_1 and Λ_2, the joint node relocates from its location in regular lattice to a random location within a circle of radius Δ (degree of irregularity).

of a wall from a unit cell. To maintain the number of walls in each unit cell, the maximum value of the randomness parameter is changing in the range of $0 \leq \Delta < 0.5$. Fig. 4 illustrates two different degrees of randomness (Δ=0.25 and 0.5) for the honeycombs. The degree of irregularity, denoted as Δ, can influence the elastic modulus, and its impact is incorporated into the modified Gibson-Ashby equation in Section 2.6 using the correction factor η.

2.6. Modified Gibson-Ashby model for FG irregular honeycombs

The standard Gibson-Ashby equation for a uniform honeycomb can relate the relative density and the relative elastic modulus as follows:

$$\frac{E_u}{E_0} = C\left(\frac{\rho_u}{\rho_0}\right)^n \tag{15}$$

in which C and n are defined as calibration parameters for a uniform honeycomb that should be fitted for a desired configuration. We propose the modified Gibson-Ashby model for FG honeycombs with a random irregularity by substituting Eqs. (8) and (12) into Eq. (15) and introducing κ and η as the correction factors for FG and random irregularity effects, respectively,

$$\frac{\bar{E}}{E_0} = \kappa\eta C\left(\frac{\bar{\rho}}{\rho_0}\right)^n \tag{16}$$

Accordingly, κ is a function f_1 of the degree of gradual changes in the wall thickness, controlled by the ratio (R_N/R_0) and the exponent m, while η is a function f_2 of the degree of randomness, Δ:

$$\kappa = f_1\left((R_N/R_0), m\right), \tag{17a}$$

$$\eta = f_2(\Delta), \tag{17b}$$

For the special case of $R_N/R_0 = 1$ or/and $m = 1$, the FG effect disappears, leading to a uniform honeycomb with κ=1. Besides, $\Delta = 0$ eliminates random irregularity resulting in η=1. The correction factor κ and η introduced here are later calibrated in Section 4 across a wide range of geometries for HEX, TRI, and SQ honeycombs.

Since the relative properties of the FG honeycombs vary in the gradation direction, x, based on Eq. (7), it makes sense to define the localized (cell by cell) version of the Gibson-Ashby equation. In order to evaluate the local relative properties, the FG correction factor is set to one (κ=1) in Eq. (16), because within each cell the aspect ratio is almost uniform. Thus, the localized form is obtained as,

$$\frac{E(x)}{E_0} = \eta C\left(\frac{\rho(x)}{\rho_0}\right)^n \tag{18}$$

2.7. FE simulations

Numerical simulations using FE analysis have been conducted with the aid of the commercial software, COMSOL Multiphysics®. Three types of FE models have been utilized as follows:

- **2D beam model**: Each wall is defined as a beam with a rectangular cross-section. The out-of-plane depth is assumed to be equal to the wall length. For uniform configurations, the in-plane beam thickness is set based on the given aspect ratio, R_u, while for the FG honeycombs the beam thickness is defined as a function of x coordinate (FG direction) so that the aspect ratio varies from the given R_0 and R_N at two sides with a power of m. For irregular models, the joints are randomly relocated based on Eq. (14). A unit cell count of $N = 20$ in both in-plane directions was selected to ensure that the results are independent of the number of unit cells, consistent with previous studies [55]. The convergence studies for the unit cell number have been detailed in Fig. S8 in **Supplementary Information File**. Each beam is discretized to 10 Timoshenko beam elements with a cubic displacement field and a quadratic rotation field. Our convergence study confirms that for 10 elements per beam, the calculated relative elastic modulus accurately converges. A sample meshed model for a uniform TRI geometry is presented in Fig. S13 in **Supplementary Information File**. This 2D beam model is used for three purposes in this study: first, the validation study of the model in Figs. 6 and 7. Second, calibration of the random irregularity correction factor η, i.e., FE results in Fig. S11 in **Supplementary Information File**. Third, the comparison study for the validity of correction factors, i.e., FEM Beam in Fig. 9. In the third case, the geometry of the model is identical to the 3D-printed samples while the walls are modeled as beam elements.
- **2D plane-stress solid model**: The 2D sketch of CAD models of 3D-printed samples (before extrusion) are used as the geometry without any modifications. The out-of-plane thickness is set to 10 mm identical to 3D-printed samples and a plane-stress condition is applied. Models are meshed by a Free triangular element with a quadratic serendipity displacement field. The convergence study is presented in Fig. S12, indicating that the calculated relative modulus converges rapidly by increasing the number of elements. An "extra fine" mesh resolution is applied to all models in COMSOL Multiphysics®. A sample meshed model of an FG-regular HEX geometry is presented in Fig. S13 in **Supplementary Information File**. The results of this FE model are solely reported in Fig. 9, as FEM Solid 2D, for the comparison study.
- **3D structural solid model**: The 3D CAD models of 3D-printed samples are used as the geometry without any modifications. The models are meshed by a Free tetrahedral element with a quadratic serendipity displacement field. An "extra fine" mesh resolution is applied to all models in COMSOL Multiphysics®. A sample meshed model of an FG-irregular SQ geometry is presented in Fig. S13 in **Supplementary Information File**. The results of this FE model are solely reported in Fig. 9, as FEM Solid 3D, for the comparison study.

To evaluate the relative elastic modulus of an FE model, we consider two sides of the model perpendicular to FG direction x. An arbitrary displacement along x is applied to the nodes on one side, while the displacement of the nodes on the other side is fixed along x direction. In addition, for the 2D beam model, the rotation of nodes on the fixed side is set to zero. The equivalent stress is determined by dividing the resultant reaction force along the x direction at the fixed nodes by the apparent cross-sectional area of the model perpendicular to the load direction. Correspondingly, the equivalent strain is obtained by dividing the applied displacement by the length of the model along the x direction. Then, the effective modulus is computed by dividing the equivalent stress by the equivalent strain.

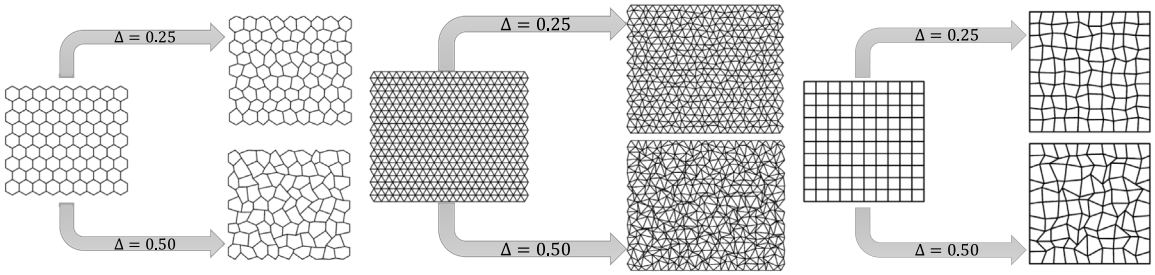

Fig. 4. Regular and irregular HEX, TRI, and SQ honeycomb structures. The degree of irregularity is controlled by varying Δ in the degree of 0 to 0.5.

Table 1
The relative density ($\bar{\rho}/\rho_0$) computed by weighting the samples and comparing them with the corresponding CAD models and analytical expression in Eq. (8).

		SQ	TRI	HEX
Eq. (8)	Uniform	0.4471	0.6910	0.2742
	FG	0.5520	0.5879	0.3549
CAD Model	Uniform	0.4082	0.5722	0.2407
	FG-Regular	0.4897	0.4871	0.3078
	FG-Irregular	0.5042	0.4905	0.3158
3D-Printed	Uniform	$0.4830 \pm .0242$	$0.6791 \pm .0340$	$0.2863 \pm .0143$
	FG-Regular	0.5813 ± 0.0291	0.5812 ± 0.0291	0.3655 ± 0.0183
	FG-Irregular	0.5990 ± 0.0230	0.5841 ± 0.0292	0.3750 ± 0.0188

3. Method

3.1. Fabrication (3D printing) of honeycombs

The honeycombs specimens were fabricated using a Stratasys J750™ 3D printer, operating in high-quality mode with a layer height resolution of 27 μm and a dimensional accuracy of 200 μm. All specimens were fabricated using Vero PureBlack™ material.

The mechanical properties of this material were determined through specific uniaxial tests following ASTM-D638 standards on the dog bone samples shows in Fig. S9. During these auxiliary tests, a constant strain rate of 0.1 mm/sec was applied to the upper cross-head of the BETA 100 loading frame machine by MESSPHYSIK. The results yielded an average elastic modulus of $E_0 = 1436 \pm 10$ MPa. Additionally, the bulk material was estimated to have a density of $\rho_0 = 1.175\,\mathrm{g/cm^3}$.

The decision to use a printer that exploits material-jetting technology was made because it allows the production of almost isotropic samples with relatively small defects [60]. For each unit cell type, three different configurations were printed, namely uniform, FG-regular, and FG-irregular, whose photographs are presented in Fig. 5. For the uniform samples, the dimensionless thickness was considered to be $R = 0.25$ and the thickness was $t = 2 \pm 0.05$ mm. For FG samples, the degree of gradation, (R_N/R_0), measured as 2.88, 2.83, and 2.83 for HEX, TRI, and SQ samples, respectively, with a linear variation, i.e., m=1. The corresponding minimum thickness values were $t_0 = 1.35 \pm 0.05$ mm for HEX and SQ and $t_0 = 0.8 \pm .05$ mm for TRI unit cells.

The dimensions of all specimens are measured as 111 ± 0.5 mm × 88 ± 0.1 mm. To determine the relative density of the printed samples, accurate weight measurements were taken prior to the compression tests. The resulting relative densities from weight data have been documented in Table 1 and compared to those obtained from the CAD models and theoretically predicted by Eq. (8). As seen in Table 1, the 3D-printed samples present slightly higher relative densities than both CAD and Eq. (8). This systematic increase is typical of material-jetting 3D printing and is caused by slight over-curing and resin bleed at wall junctions, resulting in modestly thicker effective walls than specified in the CAD model [60].

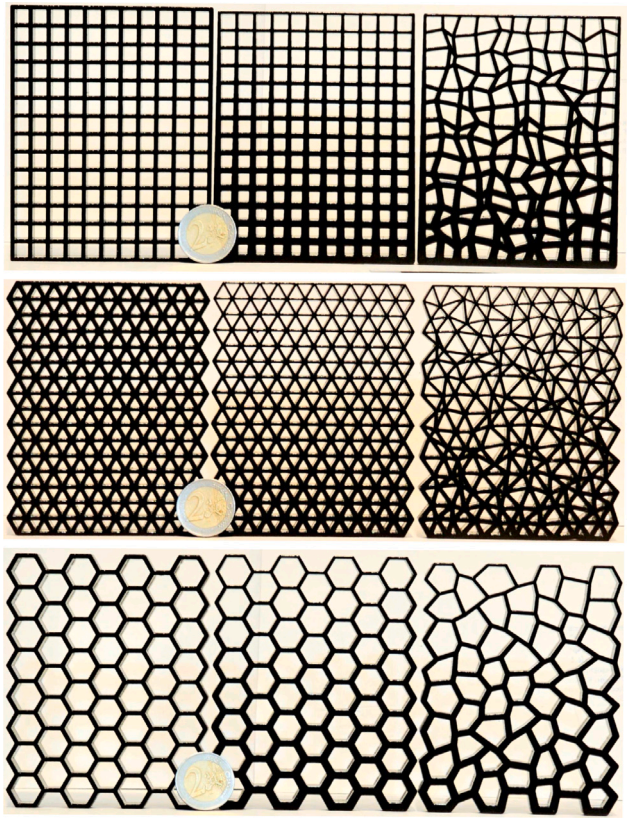

Fig. 5. 3D-printed FG specimens for experimental tests. From top to bottom: lattice structures with SQ, TRI, and HEX unit cell, from left to right: uniform, FG regular, and FG irregular.

3.2. Compression test on 3D-printed honeycombs

In order to evaluate the accuracy of the refined Gibson-Ashby model for predicting the relative elastic modulus of the FG irregular honeycombs, a series of compression tests were conducted on the 3D-printed honeycombs. The honeycombs were tested under compression load by conducting a steady strain rate of 0.1 mm/sec to the upper face of the specimens with a BETA 100 loading frame machine in order to assess the elastic modulus. Based on the ASTM-D638 guidelines, each configuration of the honeycombs was tested three times. Length changes were measured using a linear variable differential transformer mounted between the compression platens to accurately record the specimen displacement and account for machine compliance.

4. Results and discussion

This section compares the relative elastic modulus predicted by the proposed modified Gibson-Ashby model, FE numerical simulations, and

results obtained from compression tests on the 3D-printed samples. The comparison demonstrates the applicability of the correction factors in capturing the effects of graded wall thickness variation and random irregularities. Firstly, all the fitting parameters in Eq. (16) must be determined. The two parameters, C and n, from the standard form of the Gibson-Ashby equation, i.e., Eq. (15), are calibrated to the uniform regular honeycombs. To determine these parameters, a range of uniform aspect ratios R_u is introduced into Eqs. (3) and (4) to calculate the relative densities and corresponding relative elastic moduli. For HEX and SQ unit cells $0.05 \leq R_u \leq 0.5$ while for the TRI one, R_u is limited to 0.35 to avoid unrealistically high relative density values. By fitting Eq. (15) to these pairs, values of the multiplier C and the exponent n are determined, as presented in Table 2. Note that Eq. (4) is derived from structural analysis based on Timoshenko beam theory, meaning that the values of C and n are best fitted to this closed-form model.

Next, since the analytical relationship for determining the relative elastic modulus, Eq. (4), is based on the assumption of a regular periodic geometry for the honeycombs, the FE model must be utilized to assess the effects of random irregularity and to calibrate the η correction factor. For this purpose, the degree of irregularity is incrementally increased by adjusting the Δ parameter within a range of 0 to 0.5, and its impact on the equivalent elastic modulus of the honeycomb is evaluated via the FE simulations. Due to the random nature of irregularity, 20 random configurations (20 combinations of Λ_1 and Λ_2) are averaged for each value of Δ. The aspect ratio has been consistently maintained at $R_u = 0.25$ across all the models, i.e., κ=1, to isolate the effects of irregularity from the graded change in aspect ratio. Fig. S11 in **Supplementary Information File** plots the η values that fit Eq. (16) to the averaged FE results in a given Δ for all three honeycomb types. The results demonstrate that an increase in the Δ results in a dramatic decrease in the relative elastic modulus of honeycombs with SQ and TRI unit cells. For the extreme degree of irregularity with Δ=0.5, the corresponding η values are 0.868 and 0.647, for TRI and SQ honeycombs, respectively, while the HEX unit cell shows almost no clear dependency on irregularity, offering η=1. It highlights the significant softening effect of random irregularity on TRI and SQ configurations. This is because introducing random irregularities in TRI and SQ lattices alters the deformation mechanism from stretching-dominated to bending-dominated, whereas the HEX design remains bending-dominated regardless of the irregularity. A best-fitting to the observed trend for the SQ and TRI configurations is performed. The fitting function, $\eta = f_2(\Delta)$, is presented in Table 2 for TRI and SQ irregular honeycombs.

In the subsequent step, the κ correction factor is fitted for FG honeycombs. To cover a broad spectrum of grading patterns, the dimensionless wall thickness ratio, (R_N/R_0), is varied from 1 to 5, while the exponent m is set to 1, 2, and 3 to account for both linear and nonlinear variations. The effective relative density and effective relative elastic modulus are evaluated from Eqs. (8) and (12). Substituting these effective values into Eq. (16), and setting $\eta = 1$ to exclude irregularity, the correction factor κ is obtained across the range of $1 \leq (R_N/R_0) \leq 5$ for each exponent m. The calibrated κ values for HEX, TRI, and SQ lattices have been depicted in Fig. S10 in **Supplementary Information File**. In all cases, κ=1 when (R_N/R_0)=1, corresponding to uniform honeycombs, however, κ gradually decreases by increasing (R_N/R_0). It means that the classical Gibson-Ashby equation fitted on uniform honeycombs overestimates the effective relative elastic modulus for FG ones. HEX honeycombs experience the highest softening due to the FG effect. A best-fitting for $\kappa = f(R_N/R_0)$ in the form of a quintic function, as presented in Table 2, is performed for each exponent m. The unknown coefficients are provided in Table S1 in **Supplementary Information File**.

After calibrating the parameters, C, n, κ, and η, the ability of the modified model proposed in Eq. (16) to reproduce trends in relative elastic modulus under varying grading and irregularity conditions is examined. Fig. 6 displays the relationship between the relative elastic modulus and relative density for uniform honeycombs under both regular (Δ=0) and high-degree irregularity (Δ=0.5) conditions. FE simulations based on the Timoshenko beam element are provided for both cases. In addition, the analytical expression from Eqs. (5) and (6) are presented solely for the regular honeycombs. To illustrate the modified Gibson-Ashby model in Eq. (16), which assumes lattice uniformity ($R_0 = R_N = R_u$), the κ correction factor is set to 1 while the η correction factor varies depending on the honeycomb type and the degree of irregularity, indicated by the Δ value. For the regular honeycombs, we set η=1. The results show an accurate agreement between the exact expression (hollow circles), and the modified Gibson-Ashby model (solid line), confirming the accuracy of the calibrated parameters C and n to the closed-form solutions in Eq. (4). Moreover, the FE simulations for uniform structure (solid red circles) closely follow the modified Gibson-Ashby model (solid line) with a coefficient of determination, R^2, equal to 1, 0.99, and 1 for HEX, TRI, and SQ regular honeycombs, respectively. It confirms the validity of the FE numerical approach. Additionally, for honeycombs with a high degree of irregularity, Eq. (16) (dashed line) closely matches the FE results for irregular geometries (solid triangles) across the entire range of aspect ratios, confirming the accuracy of the calibrated η correction factor. The coefficient of determination, R^2, is 0.95, 0.99, and 0.96 for HEX, TRI, and SQ irregular uniform honeycombs, respectively. Note that for HEX uniform lattice solid and dashed lines coincide, since η=1. Furthermore, to illustrate the impact of irregularity on lattice stiffness, consider the case at a similar relative density (≈ 0.35). For the regular, uniform structures, the effective stiffness values are approximately 0.052, 0.131, and 0.200 for HEX, TRI, and SQ lattices, respectively (see Fig. 6). Introducing irregularities reduces these values to 0.047, 0.109, and 0.122, highlighting that HEX lattices are least affected, whereas TRI and SQ lattices experience more substantial reductions. This trend is consistent with the results shown in Fig. S11 of the supplementary data.

Fig. 7 illustrates the predicted relative elastic modulus for regular and irregular ($\Delta = 0.5$) FG honeycombs for the HEX, TRI, and SQ structures. The FE results for both regular and irregular honeycombs are plotted in this figure, while the analytical solutions are shown only for the regular structures, obtained from Eqs. (8) and (12). In addition, the classical Gibson-Ashby equation (Eq. (15), without any correction factor) and the modified version with the κ correction factor—appropriate for FG honeycombs—are included; details of the modified model are provided in Fig. S10 in the Supplementary Information. The corresponding η correction factor is also applied to the irregular honeycomb configurations. Three different cases have been considered for reporting the results: a linear ($m = 1$) gradation with a moderate change in the dimensionless thickness ($R_N/R_0 = 3$), alongside an extreme variation in the dimensionless thickness ($R_N/R_0 = 5$) with linear ($m = 1$) and non-linear ($m = 3$) functionalities. Because the same values of R_0 and R_N produce different relative densities for the three topologies according to Eq. (5), the initial points in Fig. 7 naturally differ between HEX, TRI, and SQ lattices. In all cases, the values of R_0 and R_N are

Table 2
The calibrated parameters of the modified Gibson-Ashby model in Eq. (16). The multiplier C and the exponent n are fitted to Eq. (3) and Eq. (4) for uniform honeycombs. The coefficients A_i for estimating the FG correction factor, k, are presented in Table S1 in **Supplementary Information File** for m=1, 2, and 3, best fitted to Eq. (8) and Eq. (12). The random irregularity correction factor, η, is fitted to a set of randomly irregular FE simulations for different degrees of irregularity, Δ, as detailed in Fig. S11 in **Supplementary Information File**.

	C	n	$\kappa = f_1((R_N/R_0), m)$	$\eta = f_2(\Delta)$
HEX	0.66	2.43		1
TRI	0.53	1.37	$A_0 + \sum_{p=1}^{5} A_P \left(R_N/R_0\right)^p$	$1 - 0.53\Delta^{2.01}$
SQ	0.69	1.21		$1 - 0.95\Delta^{1.43}$

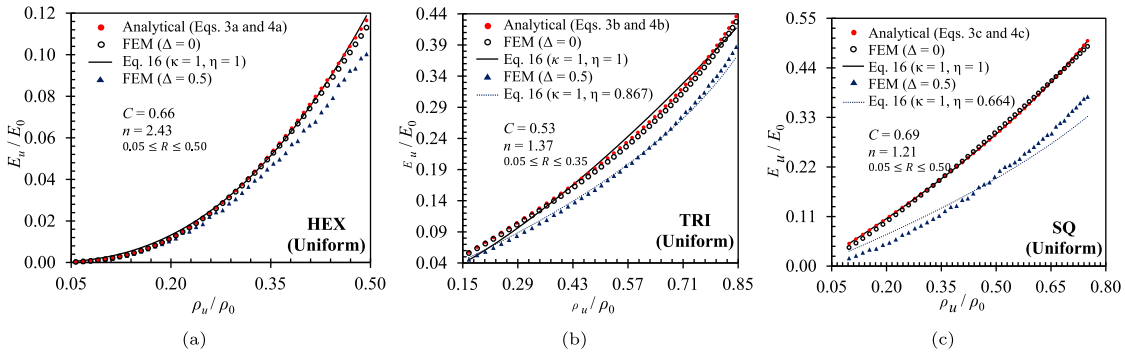

Fig. 6. The comparison between the modified Gibson-Ashby model with FE simulations for the uniform regular ($\Delta = 0$) **and irregular** ($\Delta = 0.5$) **honeycombs.** A remarkable accuracy for the calibrated multiplier C and exponent n is observed. The calibrated Gibson-Ashby model accurately fits the FE simulations for both regular and irregular uniform honeycombs.

increased proportionally to maintain a constant ratio. For the lattice structures with HEX and SQ unit cells, the minimum and maximum values of the aspect ratio are set to 0.05 and 0.5, respectively, whereas, for the TRI honeycombs, the maximum aspect ratio is set to 0.35. For regular FG honeycombs, the modified model (solid lines) closely fits the analytical expression (hollow circles), confirming the accuracy of the calibrated κ correction factor. Besides, the FE simulations based on the Timoshenko beam element for regular lattices (solid red circles) accurately follow the modified Gibson-Ashby model (solid line) with a coefficient of determination, R^2, equal to 0.99, 0.82, 0.99 for HEX, 0.97, 0.73, and 0.94 for TRI, and 1, 1, and 0.99 for SQ honeycombs for $(m, (R_N/R_0))$ pairs equal to (1, 3), (1, 5), and (3, 5), respectively. Comparing the modified model for irregular FG lattices with the FE simulations (solid triangles) illustrated an acceptable accuracy for the model. Although the κ and η correction factors are calibrated independently, the results demonstrate that the proposed modified equation with η correction factor effectively predicts the relative elastic modulus for irregular FG honeycombs across a broad spectrum of aspect ratio variations and high degrees of irregularity. The results obtained from the irregular FG lattice structure with the HEX unit cell align with those of the regular lattice structures, confirming the low sensitivity of the HEX honeycomb to the random irregularity.

Next, the accuracy of the localized (cell-by-cell) version of the Gibson-Ashby model introduced in Eq. (18) is examined. For this purpose, both the relative density along the FG honeycomb, $\rho(x)/\rho_0$, and the corresponding relative stiffness values $E(x)/E_0$ are calculated directly from Eq. (7) using the appropriate α parameter provided in Fig. S1 and Fig. S2 in **Supplementary Information File**. Subsequently, the $\rho(x)/\rho_0$ function from Eq. (7) is inserted into Eq. (18) and by incorporating the fitted values of C and n obtained from the curve-fitting on the corresponding uniform honeycomb, presented in Table 2, the value of $E(x)/E_0$ is predicted.

Fig. 8 compares the predicted values of the relative elastic modulus using the exact analytical expression and the cell-wise application of the Gibson–Ashby model introduced in Eq. (18). The local density values used along the FG direction correspond to the actual cell positions in the structure, with R_0 and R_N marking in the plots. The results confirm that this pointwise approach effectively captures the variation in elastic modulus with acceptable accuracy across the length of the functionally graded honeycomb.

Finally, to assess the effectiveness of the correction factors κ and η, nine distinct samples were designed: three uniform, three FG regular, and three FG irregular structures with HEX, TRI, and SQ topologies. These samples were 3D-printed and underwent uniaxial compression tests to determine their relative elastic modulus, as presented in the Methods section. Additionally, the corresponding FE models for these nine designs were constructed based on the exact CAD model of the printed samples. Three different FE approaches were employed: a 3D solid model, a 2D plane-stress solid model, and a Timoshenko beam model, resulting in 27 FE simulations in total. Details regarding meshing and boundary conditions are provided in the Methods section. For the given geometric parameters of the samples ($R_N/R_0 = 2.88$, 2.83, and 2.83 for the HEX, TRI, and SQ designs, respectively, and linear variation in all the samples, $m = 1$), the correction factor κ was found to be 0.67, 0.91, and 0.92 from Table 2. Given the irregularity degree of 0.5 for all the samples, the corresponding values of η were determined as 1.00, 0.87, and 0.66 from Table 2. Since these correction factors act as multipliers for the coefficient C in the Gibson-Ashby equation under a fixed exponent n, we first examined the ratio $C = (E_u/E_0)/(\rho_u/\rho_0)^n$ for the uniform structures. The experimental results from printed samples were compared with predictions from the three FE models (solid 3D, solid 2D plane-stress, and Timoshenko beam) in Fig. 9 (a-c) for HEX, TRI, and SQ configurations. In the uniform case, both κ and η are unity, meaning that these plots directly represent the coefficient C, which establishes the relationship between relative modulus and relative density. The exponent n values are replaced from fitting to analytical expressions in Eq. (3) and Eq. (4) listed in Table 2, along with the relative densities from Table 1. As observed, there are discrepancies among the C values obtained through different methods, indicating that various modeling approaches yield different estimates for the relative modulus. As expected, the FE beam and solid models diverge when the length-to-cross-sectional ratio decreases. The discrepancy between the experimental and modeled results arises from multiple factors. First, as shown in Table 1, the theoretical predictions for relative densities by Eq. (8) exhibit lower relative densities than printed specimens. Second, the Gibson-Ashby model, while effective for low-density cellular structures, becomes less accurate at higher relative densities (0.29–0.68 for 3D-printed samples), as widely documented in the literature. This limitation is inherent to the model itself. Third, the correction factors κ and η are fitted to a wide range of FG and irregular designs where a certain level of deviation in every fitting is unavoidable. Lastly, variability in the bulk material properties, particularly in 3D-printed polymers, contributes to deviations. The elastic modulus of the bulk material may differ when printed as a solid block in dogbone samples versus thin honeycomb walls due to differences in solidification conditions and defect formation. Thus, using the bulk elastic modulus from a printed solid reference sample as the denominator in relative modulus calculations introduces additional uncertainty.

Despite variations in C values for different methods in Fig. 9 (a-c), it is essential to clarify that the goal of this study is not to tune C to fit the Gibson-Ashby model to experimental data. Instead, our objective is to assess whether the analytically derived κ and numerically determined η, based on Timoshenko beam simulations, can reliably capture the effects of FG and random irregularities in both experimental and solid FE models. To evaluate this, the corresponding correction factors were applied to experimental and numerical results in Fig. 9

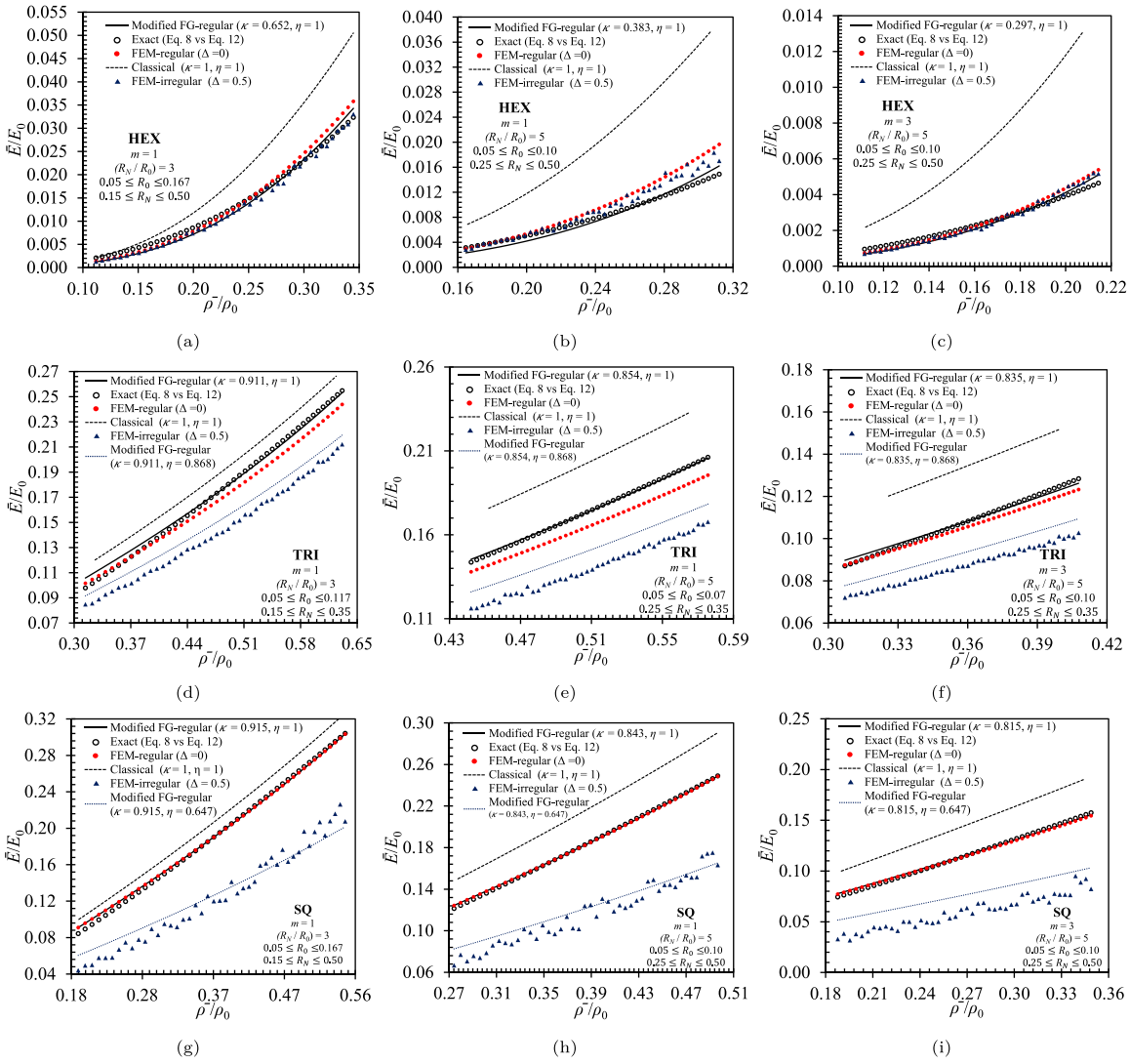

Fig. 7. The Gibson-Ashby model for the uniform regular and irregular (Δ = 0.5) honeycombs with (a-c) HEX, (d-f) TRI and (g-i) SQ unit cell. The correction factors κ and η effectively fit the modified model to the FE simulations and analytical predictions. The classical Gibson-Ashby model is plotted to highlight its significant error in elastic modulus prediction for FG irregular honeycombs.

(d-i) for HEX, TRI, and SQ structures. The results demonstrate that introducing FG architectures and random irregularities consistently reduces the proportionality coefficient in the Gibson-Ashby equation, aligning with our model's predictions, where both κ and η are less than unity. As expected, since these correction factors were calibrated based on Timoshenko beam theory, they accurately predict these effects in beam-based FE models with a maximum error of 6%. Notably, the same correction factors also provide reasonable predictions for 3D-printed samples, with a prediction error below 15%. This normalized validation format was deliberately chosen because it removes secondary experimental variability (bulk modulus, density measurement) and directly proves that the proposed κ and η factors accurately extend the classical uniform C value to real graded and irregular lattices. Therefore, it is proved that the proposed correction framework serves as a practical tool for incorporating FG architectures and random irregularities in cases where the uniform Gibson-Ashby coefficient C is available. For denser honeycombs, where the standard Gibson–Ashby model tends to underestimate stiffness, the revised formulations by [61] offer improved predictions. While our study primarily focuses on the effect of functional grading and irregularities, incorporating their correction could further enhance accuracy in the high-density regime and will be considered in future work.

The proposed κ and η correction framework suggests three main advantages. First, it preserves the conventional Gibson–Ashby power-law form and keeps the standard C and n values used for regular honeycombs, so existing material databases can be used without re-calibration. Second, the correction factors are provided as ready-to-use charts that eliminate the need for additional simulations or experiments. Third, the method improves stiffness prediction for both beam-based models and real 3D-printed specimens, even in cases with strong grading or pronounced irregularities, and its accuracy is suitable for preliminary design and certification. The main limitation is that the current charts apply only to in-plane elastic modulus of extruded 2D honeycombs loaded along the grading direction; out-of-plane loading and fully 3D lattice architectures require separate calibration. The approach is directly applicable to additively manufactured aerospace sandwich cores, automotive energy-absorbing structures, biomedical

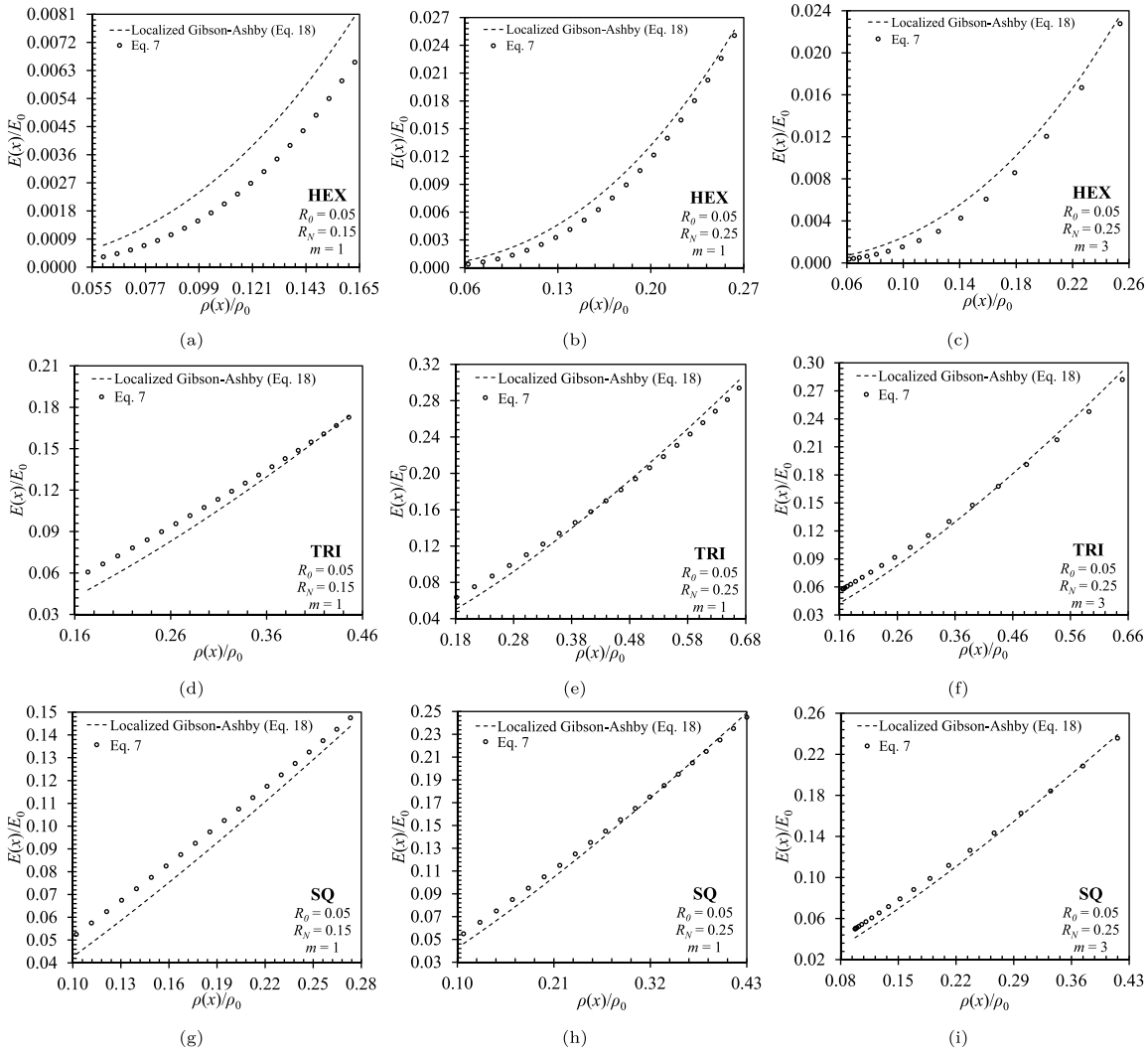

Fig. 8. The local (cell by cell) Ginson-Ashby model. Comparison between the exact expression and the Gibson-Ashby models for honeycomb with (a-c) HEX, (d-f) TRI and (g-i) SQ unit cell.

scaffolds, and lightweight protective gear, where fast and reliable stiffness estimation of imperfect graded lattices is essential for design optimization and certification workflows.

5. Conclusion

In this study, a modified model for predicting the elastic modulus of irregular FG honeycombs was developed by incorporating two correction factors into the classical Gibson-Ashby equation. These factors account for the gradual variation in wall thickness (κ) and random structural irregularities (η). Analytical approaches and FE simulations based on the Timoshenko beam theory were employed to determine these correction factors, and the accuracy of the model was validated against experimental tests on 3D-printed specimens. The results indicate that both functional grading and structural randomness lead to a reduction in the relative elastic modulus compared to uniform, periodic geometries, which are reflected in correction factors smaller than unity. More importantly, the proposed correction coefficients, although derived using the Timoshenko beam model, successfully captured the FG and irregularity effects in 3D-printed samples with a maximum error of 14.8% in experimentally measured relative elastic modulus of FG irregular samples. This highlights the effectiveness of the proposed correction framework in estimating the impact of randomness and FG variations in honeycombs by applying proper correction factors to a known uniform honeycomb modulus.

One of the key challenges in utilizing classical models such as Gibson-Ashby is their assumption of ideal, periodic structures, whereas real-world cellular materials often exhibit FG variations and irregularities. The proposed modified model bridges this gap by enabling rapid and accurate estimation of the elastic modulus without requiring extensive computational simulations or experimental testing. The proposed framework can be applied in optimizing honeycomb designs for engineering applications such as biomedical implants, impact absorption, and lightweight structures. For instance, in biomaterials, precise stiffness control in porous implants is crucial for improving mechanical compatibility with bone. Our model allows designers to estimate the effects of FG and irregularities on elastic modulus without expensive trial-and-error experiments. Although FE modeling is commonly used, this study provides a systematic approach to evaluate the combined effects of functional grading and structural irregularities on stiffness, which is less explored in the current literature. Additionally, in aerospace and automotive industries, where lightweight yet robust structures are essential, this model offers a flexible and efficient framework for early-stage evaluation of mechanical performance in functionally graded cellular structures. Overall, this study provides a practical tool for estimating the elastic modulus of complex cellular materials.

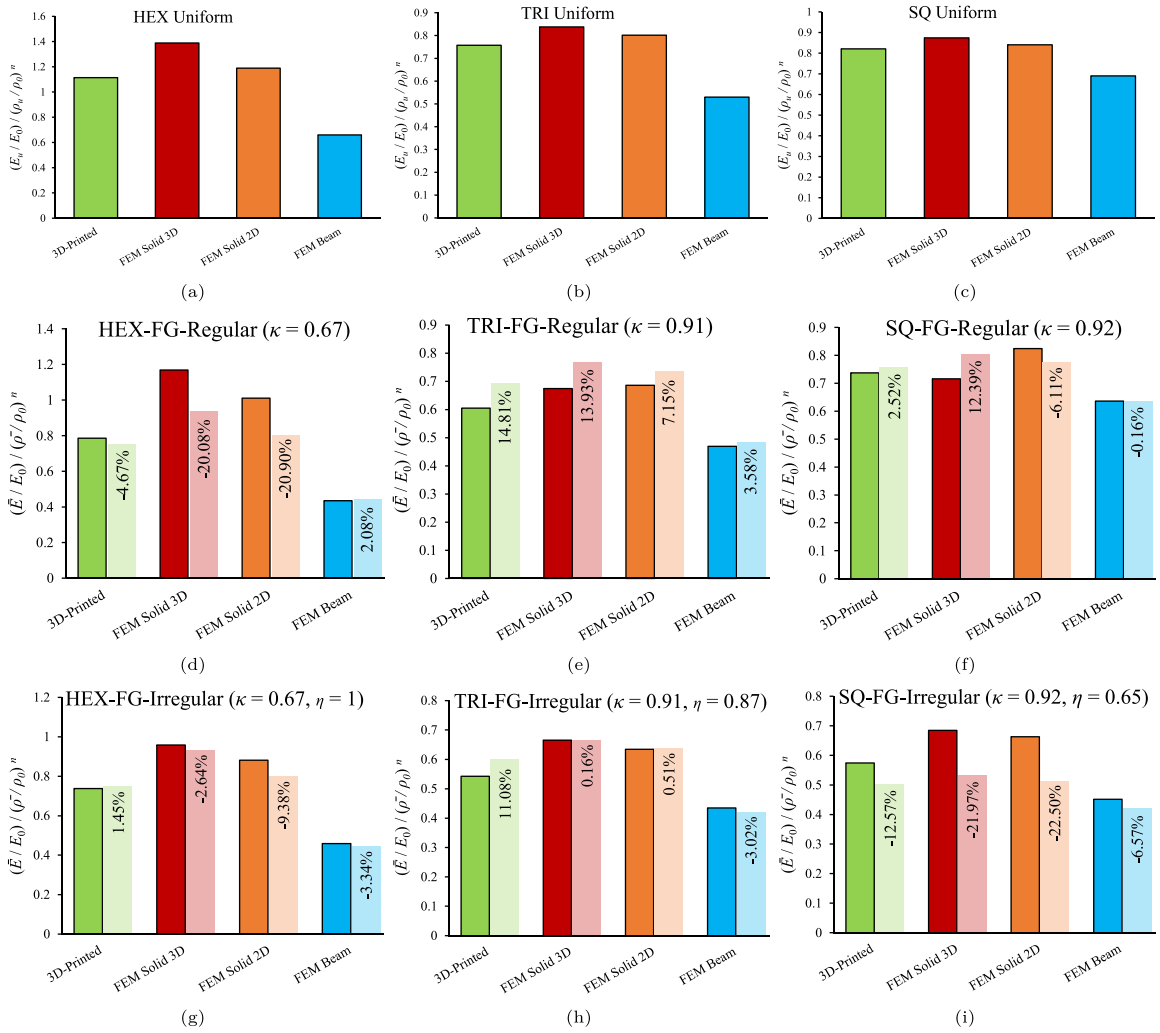

Fig. 9. The validation study of correction factors in predicting the FG and irregularity effects on the relative elastic modulus of honeycombs. (a-c) The multiple C values that fit the elastic modulus of 3D-printed and different FE simulations to the Gibson-Ashby model. (d-f) The comparison study for the accuracy of the κ correction factor for FG-regular honeycombs. (g-i) The comparison study for the accuracy of the η correction factor for FG-irregular honeycombs. Percentage errors are calculated as $100 \times |C_{\text{eff,predicted}} - C_{\text{eff,measured}}|/C_{\text{eff,measured}}$. Using this normalized form isolates the performance of the correction factors from scatter in bulk modulus and measured density, directly demonstrating that κ and η act as universal multipliers on the classical uniform C.

CRediT authorship contribution statement

M.J. Beigrezaee: Writing – review & editing, Writing – original draft, Software, Methodology, Data curation, Conceptualization. **S.K. Jalali:** Writing – review & editing, Writing – original draft, Validation, Methodology, Investigation, Formal analysis, Conceptualization. **D. Misseroni:** Writing – review & editing, Supervision, Resources, Methodology, Funding acquisition, Conceptualization. **N.M. Pugno:** Writing – review & editing, Supervision, Resources, Methodology, Funding acquisition, Conceptualization.

Funding

MJB, SKJ, and NMP are supported by the European Commission under "FRAMEGLOW" grant No. 101201568 and by the Italian Ministry of Education, University and Research (MIUR) under the PRIN-20177TTP3S.

D.M acknowledges financial support from the European Union, ERC grant HE GA 101086644 S-FOAM. Views and opinions expressed are those of the authors only and do not necessarily reflect those of the European Union or the European Research Council Executive Agency. Neither the European Union nor the granting authority can be held responsible for them.

Declaration of competing interest

The authors declare that they have no known competing financial interests or personal relationships that could have appeared to influence the work reported in this paper.

Appendix A. Supplementary data

Supplementary material related to this article can be found online at https://doi.org/10.1016/j.ijmecsci.2026.111297.

Data availability

No data was used for the research described in the article.

References

[1] Hanks Bradley, Berthel Joseph, Frecker Mary, Simpson Timothy W. Mechanical properties of additively manufactured metal lattice structures: Data review and design interface. Addit Manuf 2020;35. http://dx.doi.org/10.1016/j.addma.2020.101301.

[2] Gibson Lorna J, Ashby Michael F. Cellular solids: Structure and properties, second edition. Cellular solids: structure and properties, second edition. Cambridge University Press; 2014, p. 1–510. http://dx.doi.org/10.1017/CBO9781139878326.

[3] Bhate Dhruv. Four questions in cellular material design. Materials 2019;12(7):1060. http://dx.doi.org/10.3390/ma12071060.

[4] Qi Chang, Jiang Feng, Yang Shu. Advanced honeycomb designs for improving mechanical properties: A review. 2021, http://dx.doi.org/10.1016/j.compositesb.2021.109393.

[5] Li Yan, Feng Zuying, Hao Liang, Huang Lijing, Xin Chenxing, Wang Yushen, Bilotti Emiliano, Essa Khamis, Zhang Han, Li Zheng, Yan Feifei, Peijs Ton. A Review on Functionally Graded Materials and Structures via Additive Manufacturing: From Multi-Scale Design to Versatile Functional Properties. (6). 2020, http://dx.doi.org/10.1002/admt.201900981.

[6] Rahman Oyindamola, Uddin Kazi Zahir, Muthulingam Jeeva, Youssef George, Shen Chen, Koohbor Behrad. Density-Graded Cellular Solids: Mechanics, Fabrication, and Applications. 2022, http://dx.doi.org/10.1002/adem.202100646.

[7] Menges G, Knipschild F. Estimation of mechanical properties for rigid polyurethane foams. Polym Eng Sci 1975;15(8):623–7. http://dx.doi.org/10.1002/pen.760150810.

[8] Gibson LJ, Ashby MF. Mechanics of Three-Dimensional Cellular Materials.. Proc R Soc Lond Ser A: Math Phys Sci 1982;382(1782):43–59. http://dx.doi.org/10.1098/rspa.1982.0088.

[9] Christensen RM. Mechanics of low density materials. J Mech Phys Solids 1986;34(6):563–78. http://dx.doi.org/10.1016/0022-5096(86)90037-2.

[10] Malek Sardar, Gibson Lorna. Effective elastic properties of periodic hexagonal honeycombs. Mech Mater 2015;91:226–40. http://dx.doi.org/10.1016/j.mechmat.2015.07.008.

[11] Zhong Haozhang, Song Tingting, Li Chuanwei, Das Raj, Gu Jianfeng, Qian Ma. The Gibson-Ashby model for additively manufactured metal lattice materials: Its theoretical basis, limitations and new insights from remedies. Curr Opin Solid State Mater Sci 2023;27(3):101081. http://dx.doi.org/10.1016/j.cossms.2023.101081.

[12] Hedayati Reza, Sadighi Mojtaba, Mohammadi Aghdam Mohammad, Zadpoor Amir Abbas. Mechanical properties of additively manufactured thick honeycombs. Materials 2016;9(8):613. http://dx.doi.org/10.3390/ma9080613.

[13] Ushijima K, Cantwell WJ, Mines RAW, Tsopanos S, Smith M. An investigation into the compressive properties of stainless steel micro-lattice structures. J Sandw Struct Mater 2011;13(3):303–29. http://dx.doi.org/10.1177/1099636210380997.

[14] Yang Yunhui, Shan Meijuan, Zhao Libin, Qi Dexuan, Zhang Jianyu. Multiple strut-deformation patterns based analytical elastic modulus of sandwich BCC lattices. Mater Des 2019;181:107916. http://dx.doi.org/10.1016/j.matdes.2019.107916.

[15] Liu Yabo, Dong Zhichao, Ge Jingran, Lin Xiaohu, Liang Jun. Stiffness design of a multilayer arbitrary BCC lattice structure with face sheets. Compos Struct 2019;230:111485. http://dx.doi.org/10.1016/j.compstruct.2019.111485.

[16] Ahmadi SM, Campoli G, Amin Yavari S, Sajadi B, Wauthle R, Schrooten J, Weinans H, Zadpoor AA. Mechanical behavior of regular open-cell porous biomaterials made of diamond lattice unit cells. J Mech Behav Biomed Mater 2014;34:106–15. http://dx.doi.org/10.1016/J.JMBBM.2014.02.003.

[17] Babaee Sahab, Jahromi Babak Haghpanah, Ajdari Amin, Nayeb-Hashemi Hamid, Vaziri Ashkan. Mechanical properties of open-cell rhombic dodecahedron cellular structures. Acta Mater 2012;60(6–7):2873–85. http://dx.doi.org/10.1016/J.ACTAMAT.2012.01.052.

[18] Roberts AP, Garboczi EJ. Elastic moduli of model random three-dimensional closed-cell cellular solids. Acta Mater 2001;49(2):189–97. http://dx.doi.org/10.1016/S1359-6454(00)00314-1, arXiv:0009004.

[19] Zhong Haozhang, Das Raj, Gu Jianfeng, Qian Ma. Low-density, high-strength metal mechanical metamaterials beyond the Gibson-Ashby model. Mater Today 2023;68:96–107. http://dx.doi.org/10.1016/j.mattod.2023.07.018.

[20] Jalali Seyed Kamal, Beigrezaee Mohammad Javad, Misseroni Diego, Pugno Nicola Maria. A modified Gibson-Ashby model for functionally graded lattice structures. Mech Mater 2024;188:104822. http://dx.doi.org/10.1016/j.mechmat.2023.104822, URL https://linkinghub.elsevier.com/retrieve/pii/S0167663623002685.

[21] Ajdari Amin, Nayeb-Hashemi Hamid, Vaziri Ashkan. Dynamic crushing and energy absorption of regular, irregular and functionally graded cellular structures. Int J Solids Struct 2011;48(3–4):506–16. http://dx.doi.org/10.1016/j.ijsolstr.2010.10.018.

[22] Li Zhen, Jiang Yi, Wang Tao, Wang Liangmo, Zhuang Weichao, Liu Dan. In-plane crushing behaviors of piecewise linear graded honeycombs. Compos Struct 2019;207:425–37. http://dx.doi.org/10.1016/j.compstruct.2018.09.036.

[23] Wu Xin, Su Yutai, Shi Jing. In-plane impact resistance enhancement with a graded cell-wall angle design for auxetic metamaterials. Compos Struct 2020;247:112451. http://dx.doi.org/10.1016/j.compstruct.2020.112451.

[24] Xu Hang Hang, Luo Hui Chen, Zhang Xue Gang, Jiang Wei, Teng Xing Chi, Chen Wei Qiu, Yang Jie, Xie Yi Min, Ren Xin. Mechanical properties of aluminum foam filled re-entrant honeycomb with uniform and gradient designs. Int J Mech Sci 2023;244:108075. http://dx.doi.org/10.1016/j.ijmecsci.2022.108075.

[25] Shen CJ, Lu G, Yu TX. Dynamic behavior of graded honeycombs - A finite element study. Compos Struct 2013;98:282–93. http://dx.doi.org/10.1016/j.compstruct.2012.11.002.

[26] Duan Y, Zhao Xianhang, Du Bing, Shi Xiaopeng, Zhao Han, Hou Bing, Li Yulong. Quasi-static compressive behavior and constitutive model of graded foams. Int J Mech Sci 2020;177:105603. http://dx.doi.org/10.1016/j.ijmecsci.2020.105603.

[27] Liu Fei, Mao Zhongfa, Zhang Peng, Zhang David Z, Jiang Junjie, Ma Zhibo. Functionally graded porous scaffolds in multiple patterns: New design method, physical and mechanical properties. Mater Des 2018;160:849–60. http://dx.doi.org/10.1016/j.matdes.2018.09.053.

[28] Zhang Xiang Yu, Fang Gang, Leeflang Sander, Zadpoor Amir A, Zhou Jie. Topological design, permeability and mechanical behavior of additively manufactured functionally graded porous metallic biomaterials. Acta Biomater 2019;84:437–52. http://dx.doi.org/10.1016/j.actbio.2018.12.013.

[29] Han Changjun, Li Yan, Wang Qian, Wen Shifeng, Wei Qingsong, Yan Chunze, Hao Liang, Liu Jie, Shi Yusheng. Continuous functionally graded porous titanium scaffolds manufactured by selective laser melting for bone implants. J Mech Behav Biomed Mater 2018;80:119–27. http://dx.doi.org/10.1016/j.jmbbm.2018.01.013.

[30] Yang Lei, Mertens Raya, Ferrucci Massimiliano, Yan Chunze, Shi Yusheng, Yang Shoufeng. Continuous graded Gyroid cellular structures fabricated by selective laser melting: Design, manufacturing and mechanical properties. Mater Des 2019;162:394–404. http://dx.doi.org/10.1016/j.matdes.2018.12.007.

[31] Yi Jianjia, Burokur Shah Nawaz, Piau Gérard Pascal, De Lustrac André. 3D printed broadband transformation optics based all-dielectric microwave lenses. J Opt (United Kingdom) 2016;18(4):044010. http://dx.doi.org/10.1088/2040-8978/18/4/044010.

[32] Magnucki Krzysztof, Stasiewicz Piotr. Elastic buckling of a porous beam. J Theor Appl Mech 2004;42(4):859–68.

[33] Chen D, Yang J, Kitipornchai S. Elastic buckling and static bending of shear deformable functionally graded porous beam. Compos Struct 2015;133:54–61. http://dx.doi.org/10.1016/j.compstruct.2015.07.052.

[34] Reza Barati Mohammad, Zenkour Ashraf M. Post-buckling analysis of refined shear deformable graphene platelet reinforced beams with porosities and geometrical imperfection. Compos Struct 2017;181:194–202. http://dx.doi.org/10.1016/j.compstruct.2017.08.082.

[35] Chen Da, Yang Jie, Kitipornchai Sritawat. Free and forced vibrations of shear deformable functionally graded porous beams. Int J Mech Sci 2016;108–109:14–22. http://dx.doi.org/10.1016/j.ijmecsci.2016.01.025.

[36] Chen Da, Yang Jie, Kitipornchai Sritawat. Nonlinear vibration and postbuckling of functionally graded graphene reinforced porous nanocomposite beams. Compos Sci Technol 2017;142:235–45. http://dx.doi.org/10.1016/j.compscitech.2017.02.008.

[37] Heshmati M, Jalali SK. Effect of radially graded porosity on the free vibration behavior of circular and annular sandwich plates. Eur J Mech A Solids 2019;74:417–30. http://dx.doi.org/10.1016/j.euromechsol.2018.12.009.

[38] Jalali SK, Heshmati M. Vibration analysis of tapered circular poroelastic plates with radially graded porosity using pseudo-spectral method. Mech Mater 2020;140:103240. http://dx.doi.org/10.1016/j.mechmat.2019.103240.

[39] Wu Helong, Yang Jie, Kitipornchai Sritawat. Mechanical Analysis of Functionally Graded Porous Structures: A Review. 2020, http://dx.doi.org/10.1142/S0219455420410151.

[40] Jalali SK, Beigrezaee MJ, Pugno Nicola M. Is it always worthwhile to resolve the governing equations of plate theories for graded porosity along the thickness? Compos Struct 2021;256:112960. http://dx.doi.org/10.1016/j.compstruct.2020.112960.

[41] Jalali SK, Beigrezaee MJ, Pugno Nicola M. Reporting a misunderstanding in relating the Young's modulus to functionally graded porosity. Compos Struct 2022;281:115007. http://dx.doi.org/10.1016/j.compstruct.2021.115007.

[42] Xiong Yin-Ze, Gao Rui-Ning, Zhang Hang, Dong Lan-Lan, Li Jian-Tao, Li Xiang. Rationally designed functionally graded porous Ti6Al4V scaffolds with high strength and toughness built via selective laser melting for load-bearing orthopedic applications. J Mech Behav Biomed Mater 2020;104:103673.

[43] Rho Jae Young, Ashman Richard B, Turner Charles H. Young's modulus of trabecular and cortical bone material: ultrasonic and microtensile measurements. J Biomech 1993;26(2):111–9.

[44] Wang Xianke, Chen Xiaohan, Huang Bin, Chen Lin, Fang Changhua, Ma Xinxin, Fei Benhua. Gradient changes in fiber bundle content and mechanical properties lead to asymmetric bending of bamboo. Constr Build Mater 2023;395:132328.

[45] Galehdari Seyed Ali, Kadkhodayan Mehran, Hadidi-Moud Saeid. Low velocity impact and quasi-static in-plane loading on a graded honeycomb structure; experimental, analytical and numerical study. Aerosp Sci Technol 2015;47:425–33.

[46] Qin Ruixian, Zhou Junxian, Chen Bingzhi. Crashworthiness design and multiobjective optimization for hexagon honeycomb structure with functionally graded thickness. Adv Mater Sci Eng 2019;2019(1):8938696.

[47] Zhao Chang, Zhou Li, Qiu Tao. Mechanical properties of jujube core shaped double-layer deformable honeycomb. Mech Adv Mater Struct 2025;1–14.

[48] Heshmati Mahmood, Jalali S Kamal, Pugno Nicola M. An innovative hierarchical design of hybrid meta-structures for longitudinal waveguides. Int J Mech Sci 2025;287:109963.

[49] Ajdari A, Canavan P, Nayeb-Hashemi H, Warner G. Mechanical properties of functionally graded 2-D cellular structures: A finite element simulation. Mater Sci Eng A 2009;499(1–2):434–9. http://dx.doi.org/10.1016/j.msea.2008.08.040.
[50] Mukhopadhyay T, Adhikari S. Equivalent in-plane elastic properties of irregular honeycombs: An analytical approach. Int J Solids Struct 2016;91:169–84. http://dx.doi.org/10.1016/j.ijsolstr.2015.12.006.
[51] Alkhader M, Vural M. Mechanical response of cellular solids: Role of cellular topology and microstructural irregularity. Internat J Engrg Sci 2008;46(10):1035–51. http://dx.doi.org/10.1016/j.ijengsci.2008.03.012.
[52] Sotomayor Oscar E, Tippur Hareesh V. Role of cell regularity and relative density on elasto-plastic compression response of random honeycombs generated using Voronoi diagrams. Int J Solids Struct 2014;51(21–22):3776–86. http://dx.doi.org/10.1016/j.ijsolstr.2014.07.009.
[53] Lipperman Fabian, Ryvkin Michael, Fuchs Moshe B. Nucleation of cracks in two-dimensional periodic cellular materials. Comput Mech 2007;39(2):127–39. http://dx.doi.org/10.1007/s00466-005-0014-9.
[54] Lipperman Fabian, Ryvkin Michael, Fuchs Moshe B. Fracture toughness of two-dimensional cellular material with periodic microstructure. Int J Fract 2007;146(4):279–90. http://dx.doi.org/10.1007/s10704-007-9171-5.
[55] Gu Huaiyuan, Pavier Martyn, Shterenlikht Anton. Experimental study of modulus, strength and toughness of 2D triangular lattices. Int J Solids Struct 2018;152–153:207–16. http://dx.doi.org/10.1016/j.ijsolstr.2018.06.028.
[56] León-Becerra Juan, González-Estrada Octavio A, Quiroga Jabid. Effect of Relative Density in In-Plane Mechanical Properties of Common 3D-Printed Polylactic Acid Lattice Structures. ACS Omega 2021;6(44):29830–8. http://dx.doi.org/10.1021/acsomega.1c04295.
[57] Van Der Burg MWD D, Shulmeister V, Van Der Geissen E, Marissen R. On the Linear Elastic Properties of Regular and Random Open-Cell Foam Models. J Cell Plast 1997;33(1):31–54. http://dx.doi.org/10.1177/0021955X9703300103.
[58] Chen C, Fleck NA. Size effects in the constrained deformation of metallic foams. J Mech Phys Solids 2002;50(5):955–77. http://dx.doi.org/10.1016/S0022-5096(01)00128-4.
[59] Chen C, Lu TJ, Fleck NA. Effect of imperfections on the yielding of two-dimensional foams. J Mech Phys Solids 1999;47(11):2235–72. http://dx.doi.org/10.1016/S0022-5096(99)00030-7.
[60] Mora Samantha, Pugno Nicola M, Misseroni Diego. 3D printed architected lattice structures by material jetting. Mater Today 2022. http://dx.doi.org/10.1016/j.mattod.2022.05.008.
[61] Malek Sardar, Gibson Lorna. Effective elastic properties of periodic hexagonal honeycombs. Mech Mater 2015;91:226–40. http://dx.doi.org/10.1016/j.mechmat.2015.07.008, URL https://www.sciencedirect.com/science/article/pii/S0167663615001568.